ChemComm

HIGHLIGHT

View Article Online
View Journal | View Issue

Check for updates

Cite this: *Chem. Commun.*, 2024, **60**, 2716

Visual monitoring of biocatalytic processes using small molecular fluorescent probes: strategies-mechanisms-applications

Guang Chen,[a] Jie Xu,[a] Siyue Ma,[a] Xinrui Ji,*[c] Jared B. Carney,[d] Chao Wang,[a] Xiaoyong Gao,[e] Pu Chen,[c] Baolei Fan,*[b] Ji Chen,[e] Yanfeng Yue *[d] and Tony D. James *[fg]

Real-time monitoring of biocatalytic-based processes is significantly improved and simplified when they can be visualized. Visual monitoring can be achieved by integrating a fluorescent unit with the biocatalyst. Herein, we outline the design strategies of fluorescent probes for monitoring biocatalysis: (1) probes for monitoring biocatalytic transfer: γ-glutamine is linked to the fluorophore as both a recognition group and for intramolecular charge transfer (ICT) inhibition; the probe is initially in an off state and is activated *via* the transfer of the γ-glutamine group and the release of the free amino group, which results in restoration of the "Donor–π–Acceptor" (D–π–A) system and fluorescence recovery. (2) Probes for monitoring biocatalytic oxidation: a propylamine is connected to the fluorophore as a recognition group, which cages the hydroxyl group, leading to the inhibition of ICT; propylamine is oxidized and subsequently β-elimination occurs, resulting in exposure of the hydroxyl group and fluorescence recovery. (3) Probes for monitoring biocatalytic reduction: a nitro group attached to a fluorophore as a fluorescence quenching group, this is converted to an amino group by catalytic reduction, resulting in fluorescence recovery. (4) Probes for monitoring biocatalytic hydrolysis: β-D-galactopyranoside or phosphate acts as a recognition group attached to hydroxyl groups of the fluorophore; the subsequent biocatalytic hydrolysis reaction releases the hydroxyl group resulting in fluorescence recovery. Following these 4 mechanisms, fluorophores including cyanine, coumarin, rhodamine, and Nile-red, have been used to develop systems for monitoring biocatalytic reactions. We anticipate that these strategies will result in systems able to rapidly diagnose and facilitate the treatment of serious diseases.

Received 15th November 2023,
Accepted 24th January 2024

DOI: 10.1039/d3cc05626k

rsc.li/chemcomm

Open Access Article. Published on 14 February 2024. Downloaded on 2/5/2026 3:32:46 PM.
This article is licensed under a Creative Commons Attribution 3.0 Unported Licence.

Introduction

Biocatalysis accelerates the transformation of substances in the body. Enzymes involved in biocatalysis are divided into oxidoreductases, transferases, hydrolases, lyases, isomerases, and ligases. While, many molecular fluorescent probes for biocatalytic processes have been developed, with this highlight we will concentrate on four important types of probes associated with cancer and aging: (1) biocatalytic transfer reactions: the γ-glutamine group is catalytically transferred from glutathione (GSH) to an amino acceptor. This reaction regulates GSH levels and cellular oxidative stress. Transferases are also important enzymes involved in tumour expression.[1,2] (2) Biocatalytic oxidation reactions: monoamines and exogenous drugs are catalytically oxidized and then inactivated. This process is involved in drug metabolism and maintains the homeostasis of neurotransmitters, and has also been found to be associated with age-related neurological diseases.[3] (3) Biocatalytic reduction reactions: under anoxic conditions, nitro compounds are reduced. This process is often used to assess the hypoxic state of cells and diagnose diseases such as cancer.[4–6] (4) Biocatalytic hydrolysis reactions: β-galactoside produces galactose through biocatalytic hydrolysis. This reaction is

[a] *The Youth Innovation Team of Shaanxi Universities, Shaanxi Key Laboratory of Chemical Additives for Industry, College of Chemistry and Chemical Engineering, Shaanxi University of Science & Technology, Xi'an, 710021, China*
[b] *Hubei University of Science and Technology, No. 88, Xianning Avenue, Xianan District, Xianning 437000, China. E-mail: fanb1980@163.com*
[c] *Department of Chemical Engineering and Waterloo Institute for Nanotechnology, University of Waterloo, 200 University Avenue West, Waterloo, Ontario N2L 3G1, Canada. E-mail: X62ji@uwaterloo.ca*
[d] *Department of Chemistry, Delaware State University, Dover, Delaware 19901, USA. E-mail: yyue@desu.edu*
[e] *Jiangsu Simba Biological Medicine Co., Ltd. Gaogang Distrct Qidizhihui Park, Taizhou City, China*
[f] *Department of Chemistry, University of Bath, Bath BA2 7AY, UK. E-mail: t.d.james@bath.ac.uk*
[g] *School of Chemistry and Chemical Engineering, Henan Normal University, Xinxiang 453007, China*

 This journal is © The Royal Society of Chemistry 2024

Open Access Article. Published on 14 February 2024. Downloaded on 2/5/2026 3:32:46 PM. This article is licensed under a Creative Commons Attribution 3.0 Unported Licence.

used for the diagnosis and detection of tumours as well as the detection of senescent cells.[7–9]

Given the significant role that biocatalysis plays in biological systems, visual detection is a particularly useful approach since it facilitates the facile evaluation of biomechanisms and the kinetics of biological process. Moreover, the development of visible molecular tools is essential for rapid disease diagnosis and treatment. Although bioanalytical techniques including colorimetric and electrochemical methods, *etc.*, are widely used for bioanalysis, these techniques lack the advantages of real-time visualization *in situ*.[10–12] As such, it is important to find a visible method for *in situ* biocatalysis monitoring. In recent years, fluorescence imaging technologies have been shown to exhibit sensitive and fast response, enabling visible real-time bioanalysis. Kovačević *et al.* and Li *et al.* have used fluorescent protein labelling and a metal organic framework (MOF) nanosheet sensor to detect biocatalytic glucose oxidation.[13,14]

While Huang *et al.* have developed the first monoamine oxidases (MAO)-A-specific two-photon fluorogenic probe.[15] Due to their unique properties, fluorescent probes for the analysis of biocatalysts have been rapidly developed. As such it is now appropriate to summarize the strategies and working mechanisms for these probes and to highlight representative fluorescent probes for the visual detection of biocatalysis (Fig. 1). In addition we have separated them into 4 categories according to the types of biocatalytic reaction involved. Design strategies, working mechanisms, and biological applications are: (1) probes for biocatalytic transfer: amino, γ-glutamine or glucoside are used as the recognition group that is linked to the fluorophore. The fluorophore can be cyanine, naphthalimide, anthracene derivatives and indole-quinolines. For example, with an amine, when the probe is activated by the biocatalyst, a carbonyl group is formed, creating a ''Donor–π–Acceptor'' (D–π–A) system, and a fluorescence output. Similarly, after the biocatalytic transfer of the γ-glutamine group, the amino group is released. Thus, the ''D–π–A'' effect of the probe is increased, thereby resulting in enhanced fluorescence. (2) Probes for biocatalytic oxidation: glucose, tyrosine or propylamine can be used as biocatalytic recognition sites, with fluorophores including cyanine, rhodamine and nano-quantum dots. The fluorescence mechanism includes the H_2O_2 assisted strategy (H_2O_2 generated during the biocatalytic process can enhance/suppress the luminescence of nano-quantum dots), and the switch of intramolecular charge transfer (ICT) (before and after the process, hydroxyl groups are caged and released, leading to enhancement of ICT and fluorescence recovery). (3) Probes for biocatalytic reduction: involving nitro/*p*-nitrobenzyl group and azo groups integrated with cyanine, BODIPY, Nile-red or naphthalimide cores. For example, when a nitro group is reduced to an amino group, fluorescence is restored due to the removal of the quenching effect by the nitro group; similarly, when a *p*-nitrobenzyl group is reduced, a 1,6-rearrangement elimination occurs, which results in the recovery of fluorescence. Similarly, when the azo group is specifically reduced to an amino group the ICT process from the amino group (D) to the fluorophore (A) is enabled, resulting in enhanced fluorescence emission. (4) Probes for biocatalytic hydrolysis: where galactoside or phosphate moieties are added to fluorophores including BODIPY, naphthalimide and natural quercetin. Here, when biocatalytic hydrolysis occurs, the galactopyranoside or the phosphate group is removed, releasing the hydroxyl group, and enhancing electron-donation to the fluorophore, resulting in fluorescence recovery. In summary, we have compiled probe construction strategies based on various fluorescent groups such as rhodamine, naphthalimide, Nile red, BODIPY and cyanine for the visualization of 4 classes of biocatalysts. Among them, rhodamine, naphthalimide, Nile red and BODIPY are widely used since these fluorophores are easily modified. However, the shorter emission wavelength limits the biological visualization application of these fluorophores. Therefore, as a near-infrared (NIR) dye, cyanine can break this limitation by enabling deeper tissue penetration. These probes play important roles in monitoring biological processes. As such, we anticipate that such probes will contribute to a deeper understanding of biocatalysis in biomedicine.

Biocatalytic transfer

Transferases are one of the six main enzymes that play an important role in living organisms. Here we used γ-glutamyl transpeptidase (GGT) as an example. GSH as an endogenous antioxidant and can regulate the oxidative stress state of cells. Cysteine is an essential amino acid in protein synthesis *in vivo* and plays an important role in the proliferation and metastasis of cancer cells. GGT has been found to be significantly enhanced in ovarian cancer, cervical cancer, liver cancer and other malignant tumours. Therefore, GGT is a suitable biomarker for tumour diagnosis. Visual monitoring of this process enables exploration of the catalytic mechanism and facilitates the diagnosis and prevention of clinical diseases.

Biocatalytic transamination

Chiral amines are important molecules widely used in the chemical industry.[16] Synthetic methods for chiral amines using ω-transaminase (ω-TA) have become particularly important due to the green synthetic credentials of the process. Therefore, it is necessary to develop an efficient biocatalytic screening platform for large-scale industrial production of chiral amines.[17–19] ω-TA relies on pyridoxal phosphate (PLP) to achieve transamination. The probe is composed of an amino group, electron-donating groups and a π-conjugated group which is the linker. When the probe is catalyzed by ω-TA, the amino group is transferred to the PLP, and the probe is converted into a carbonyl group. Therefore, a D–π–A structure is formed between the electron-donating group (D) and carbonyl (A) which results in enhanced fluorescence (Fig. 2).

Based on this strategy, Wang *et al.* developed probe **1** for the efficient screening of transamination biocatalysts (Fig. 3).[20] Probe **1** uses a naphthalene as the fluorophore, and the propan-2-amino group as the recognition group. Once probe **1** is recognized by ω-TA, the amino group is transferred to PLP, followed by the formation of a carbonyl group. Thus, the ''D–π–A'' interaction of a

Open Access Article. Published on 14 February 2024. Downloaded on 2/5/2026 3:32:46 PM.
This article is licensed under a Creative Commons Attribution 3.0 Unported Licence.

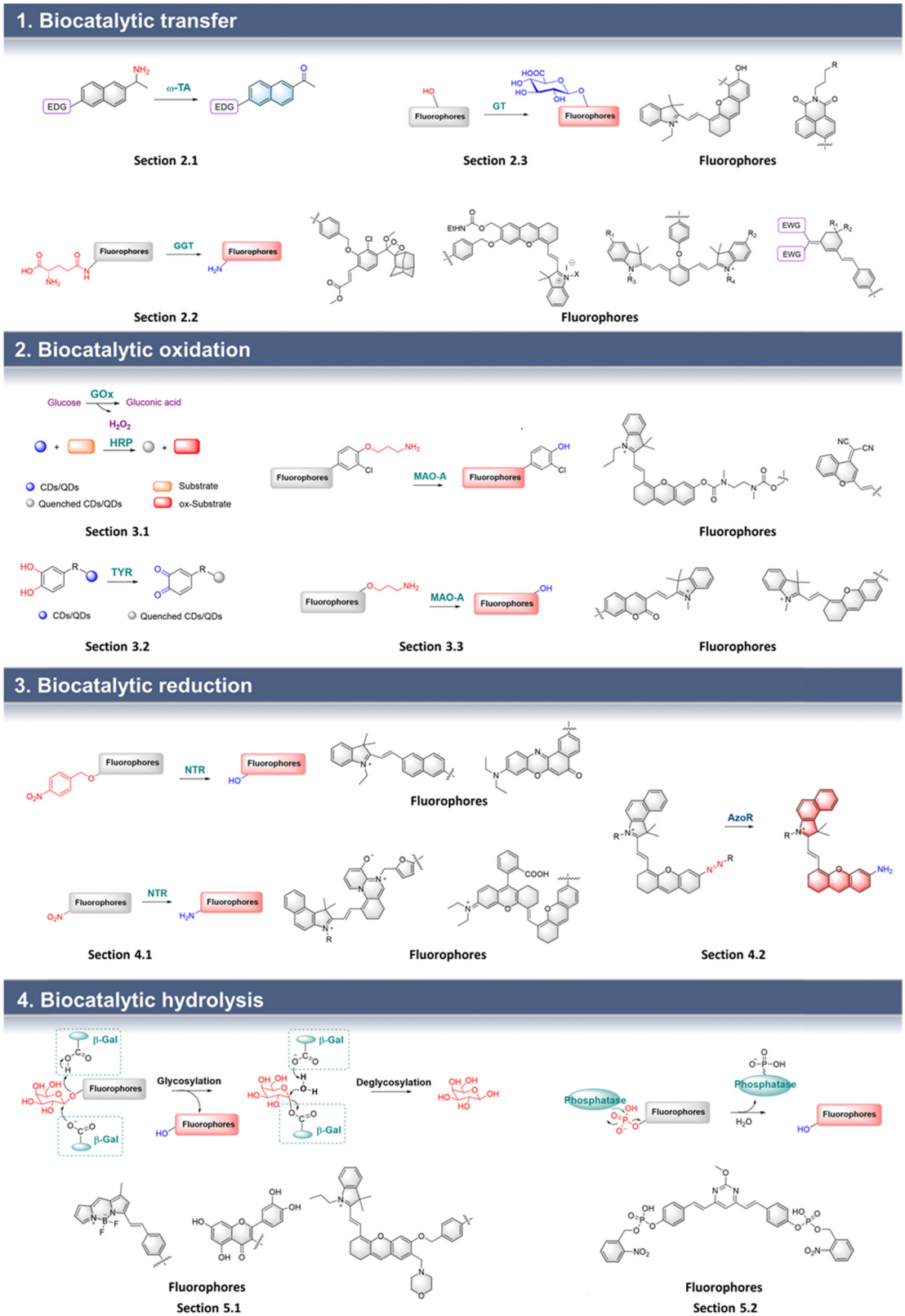

Fig. 1 Fluorescent probes for biocatalysts.

carbonyl group and an amino group occurs, resulting in the formation of fluorescent **AN**. Therefore, the efficient screening of ω-TA can be achieved by the monitoring of **AN** fluorescence emission. Probe **1** exhibits the advantages of low background

 This journal is © The Royal Society of Chemistry 2024

Open Access Article. Published on 14 February 2024. Downloaded on 2/5/2026 3:32:46 PM.
This article is licensed under a Creative Commons Attribution 3.0 Unported Licence.

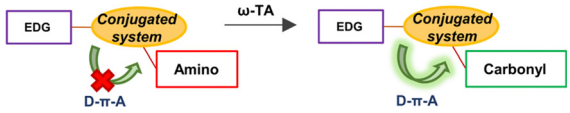

Fig. 2 Schematic diagram of "D–π–A" structure fluorophore used for detecting biocatalytic transamination.

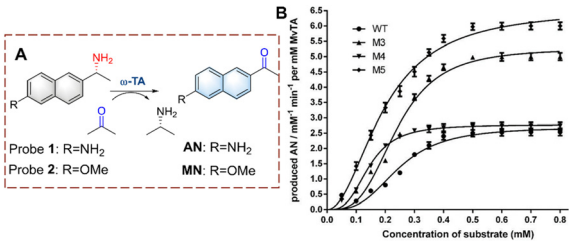

Fig. 3 (A) The structure and response mechanism of probe **1** and probe **2**. (B) Kinetic curves of wild-type and variants characterized by probe **1** (0–0.8 mM) (reprinted with permission from ref. 20 Copyright © 2020, Springer Nature).

interference, high sensitivity, and wide dynamic range. Therefore, probe **1** was used for the efficient screening of ω-TA variants, where variant M5 was shown to exhibit 3.2 times enhanced biocatalytic activity. In addition, the remarkable activity of M5 makes it a potential biocatalyst for the synthesis of (R)-amines.

A similar structure was used by Fessner *et al.* to develop probe **2** for high throughput detection (Fig. 3).[21] When probe **2** is biocatalyzed, a carbonyl group is generated, resulting in the formation of a new "D–π–A" structure, which in turn causes **MN** to fluoresce. Probe **2** was used to evaluate the biocatalytic process.

Biocatalytic glutamine transfer

GGT can transfer the γ-glutamine group from GSH to water, amino acids and peptides.[22] It has been shown to be overexpressed in cancer cells. As such, the visual detection of biocatalytic γ-glutamine transfer is useful for the diagnosis and treatment of cancer.[23–26] With these probes, the γ-glutamine group acts as the recognition group, and the fluorophore is attached either directly or using a linker.

The γ-glutamine can usually be directly attached to fluorophores, using N atoms serving as both fluorescent and recognition groups, participating in both the biocatalytic recognition

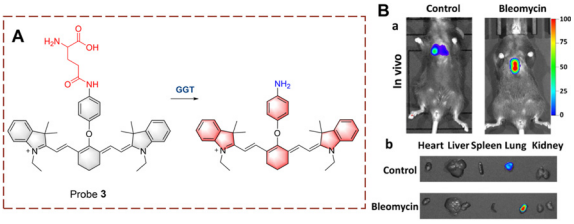

Fig. 4 (A) The structure and response mechanism of probe **3**. (B) (a) Images of probe **3** (100 μM, 30 min) in pulmonary fibrosis (bleomycin) and normal mice (control). (b) Images of isolated organs in (a) (reprinted with permission from ref. 27 Copyright © 2020, Elsevier).

and changes in fluorescence signals. The probe is non-fluorescent due to the caging by the γ-glutamine group. Subsequently, the glutamine group is recognized and cleaved by GGT, and the amino group is exposed, resulting in a significant fluorescence response.

Using this strategy, Lv *et al.* developed probe **3** for monitoring biocatalytic glutamine transfer *in vivo* (Fig. 4).[27] The cyanine fluorophore of probe **3** is a NIR dye and exhibits the advantages of reducing background interference and enables the deep penetration of tissues. The γ-glutamine group was added to cage the amine of cyanine. Therefore, the fluorescence of probe **3** is quenched. When probe **3** is recognized by GGT, the γ-glutamine group is transferred, thereby releasing the amino group, resulting in the recovery of the fluorescence. Since probe **3** exhibited a rapid and selective response it was suitable for imaging pulmonary fibrosis cells in mice and confirmed that the expression levels of GGT were directly related to pulmonary fibrosis. Therefore, providing visual evidence for research on the pathogenesis of idiopathic pulmonary fibrosis.

Kong *et al.* developed probe **4** for the visual tracking of endogenous GGT *in vivo* (Fig. 5).[28] The structure of probe **4** is 2-(3,5,5-trimethylcyclohex-2-en-1-ylidene)malononitrile, linked to a benzene through a C=C bond. A γ-glutamine group is attached as the recognition group. Probe **4** is non-fluorescent because both the cyano and γ-glutamine groups are electron-withdrawing groups. However, when the γ-glutamine group is transferred, and the amino group is released as a donor (D). Thus, probe **4** exhibits strong fluorescence due to the release of the "D–π–A" interaction, in which the cyano group acts as electron acceptor (A). Probe **4** has the advantages of large Stokes shift (213 nm), high sensitivity (LOD = 0.024 U L^{-1}), high specificity, high imaging resolution and low biological toxicity. Due to these advantages, probe **4** was used for the real-time imaging of GGT in tumour-bearing mice. Providing an effective fluorescence tool for pathological research and diagnosis of GGT-related diseases *in vivo*.

Similarly, Peng *et al.* developed probe **5** (Fig. 5).[29] Probe **5** consists of a conjugated 2-dicyanomethylene-3-cyano-4,5,5-trimethyl-2,5-dihydrofuran (TCF).[30] And the γ-glutamine group is directly attached to the core *via* an amine. Since both the cyano and γ-glutamine are electron-withdrawing groups, the fluorescence of probe **5** is in an off state. When probe **5** is recognized and undergoes biocatalysis by GGT, an amino group is generated. As such probe **5** emits fluorescence due to the released "D–π–A" interaction. In addition, probe **5** exhibits low detection limit (0.014 mU mL^{-1}) and fast response (T_e = 14 min). Probe **5** was used to distinguish normal cells from cancer cells, therefore, providing visual guidance for clinical tumour resection.

In addition, using a linker to connect the γ-glutamine group and fluorophores reduces the steric hindrance of the probe and facilitates the interaction between the probe and the enzyme, which is hindered when the receptor is directly connected. Due to a covalent connection between the linker and the phenolic group of the fluorophore the hydroxyl groups are caged and the fluorescence is quenched. However, when the recognition

Open Access Article. Published on 14 February 2024. Downloaded on 2/5/2026 3:32:46 PM.
This article is licensed under a Creative Commons Attribution 3.0 Unported Licence.

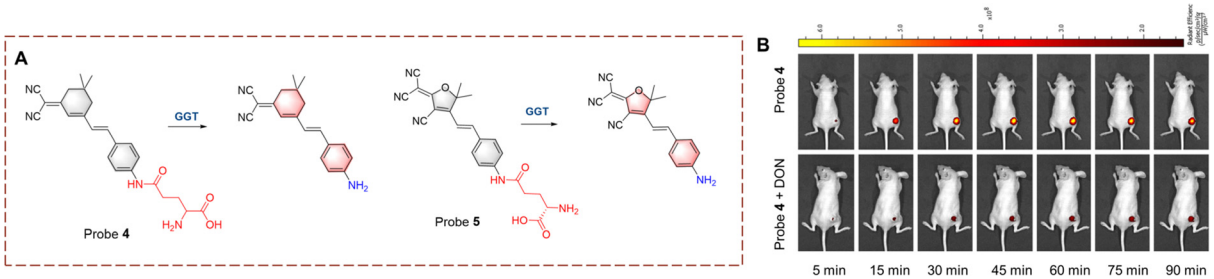

Fig. 5 (A) The structure and response mechanism of probe **4** and probe **5**. (B) Image of probe **4** (50 μM) or DON (GGT inhibitor, 2 mM) before probe **4** (50 μM) in HepG-2 tumour bearing mice (reprinted with permission from ref. 28 Copyright © 2019, Elsevier).

group is triggered, the linker also detaches, and the probe exhibits bright fluorescence, enabling the visualization of the biocatalytic process.

Inspired by the above strategy, Xie *et al.* developed probe **6** for the monitoring of the glutamine transfer reaction (Fig. 6).[31] Probe **6** is non-fluorescent due to the **HD** being caged (locked) by *p*-aminobenzyl alcohol (PABA). PABA is a self-immolative linker that reduces the steric hindrance between probe **6** and GGT, while also enabling the release of activated fluorophores. When probe **6** undergoes biocatalytic transfer, the γ-glutamine is cleaved, resulting in exposure of the amino group. Subsequently, PABA undergoes 1,6-elimination generating intermediate (**6-I**). This intermediate is unstable and converts into (**6-II**) by the release of the ethyl carbamate. Subsequently, intermediate (**6-II**) is attacked by a nucleophilic residue of GGT, and covalently immobilized and the fluorescence signal is turned on. Compared with other small molecule probes, probe **6** reduces the impact of diffusion phenomenon, thus significantly enhancing the sensitivity. As such, probe **6** could be used for the real-time imaging of HepG-2 cells and tumour-bearing mice.

Ye *et al.* have also used PABA as a linker to synthesize probe **7** based on Schaap's phenoxy-dioxetane (Fig. 7).[32] Similarly, the large fluorophore Schaap's phenoxy dioxetane is kept an appropriate distance from the active site of GGT by the PABA linker. When the γ-glutamine group is transferred, PABA within (**7-I**) undergoes self-elimination generating intermediates (**7-II**). **7-II** then undergoes chemiexcitation to generate (**7-III**) and chemiluminescence. Probe **7** exhibits the advantages of low detection limit (16 mU L^{-1}) and high fluorescence turn-on (876-fold). Due to the obvious luminescence change of probe **7**, it has been used for the detection of cancer in mice.

Guo *et al.* synthesized probe **8** with dipeptide-linker, fluorophore and γ-glutamine (Fig. 8).[33] Probe **8** is based on the indole-quinoline (QI) with a C=C bond to enhance the ICT effect. L-Proline-glycine (Pro-Gly) acts a linker, which improves stability of probe **8**. Probe **8** was initially non-fluorescent due to caging by the Pro-Gly. Once the γ-glutamine of probe **8** is transferred, the self-cyclization of Pro-Gly is rapid and releases HQI resulting in fluorescence recovery. Probe **8** was shown to target the nucleolus and inhibit RNA Polymerase I transcription. As such probe **8** is a bifunctional molecule suitable for detection and treatment. Probe **8** also provides a new strategy for development of a nucleolar targeted fluorescent probe.

Given that probes for *in vivo* monitoring suffer from inaccurate imaging due to irregular distribution, ratiometric probes have been developed to overcome differences in concentration suitable for monitoring the transamination reaction. Changes in the electron distribution of the probe, results in a red

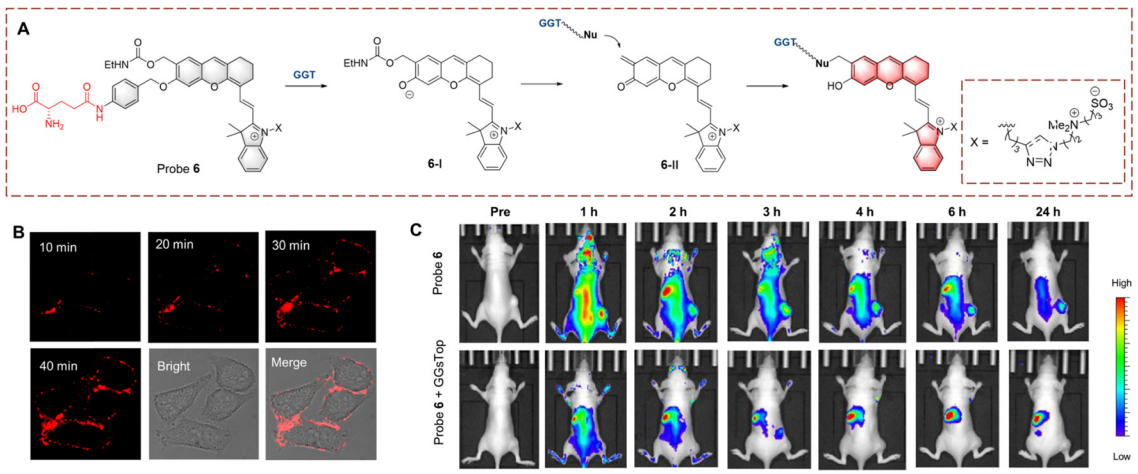

Fig. 6 (A) The structure and response mechanism of probe **6**. (B) Fluorescence image of probe **6** (1 μM) in HepG-2 cells. (C) Images of probe **6** or probe **6** with GGsTop (GGT inhibitor, 5 mM) in U87MG tumour bearing mice (reprinted with permission from ref. 31 Copyright © 2020, American Chemical Society).

 This journal is © The Royal Society of Chemistry 2024

Open Access Article. Published on 14 February 2024. Downloaded on 2/5/2026 3:32:46 PM.
This article is licensed under a Creative Commons Attribution 3.0 Unported Licence.

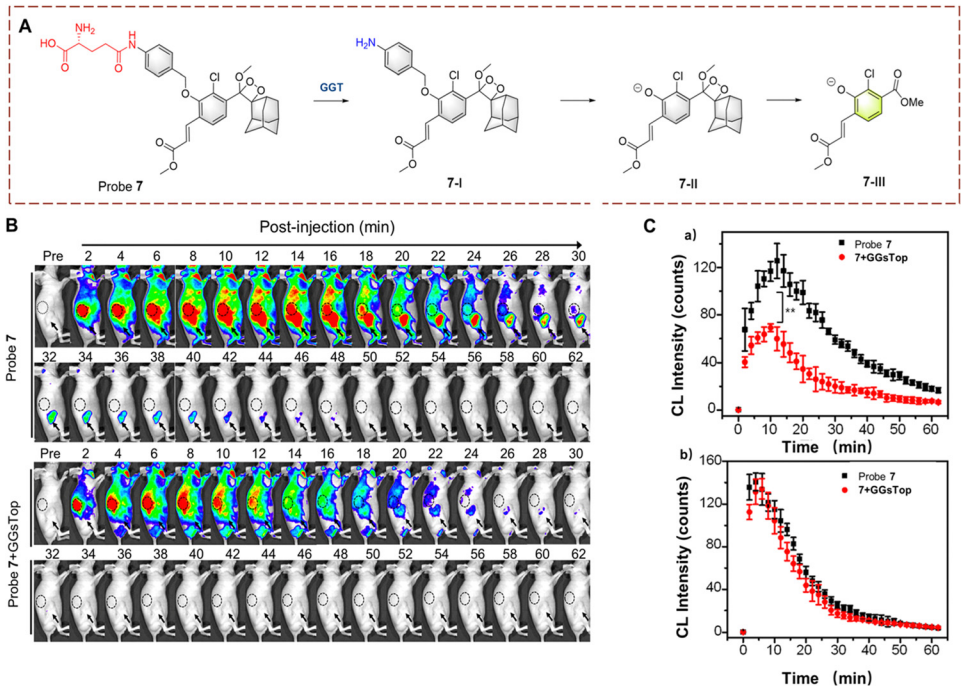

Fig. 7 (A) The structure and response mechanism of probe **7**. (B) Fluorescence images of probe **7** (100 μM) or probe **7** (100 μM) with GGsTop (10 mM) in U87MG tumour bearing mice. (C) CL intensity curve of tumour (a) and kidney (b) in figure (B) (reprinted with permission from ref. 32 Copyright © 2019, American Chemical Society).

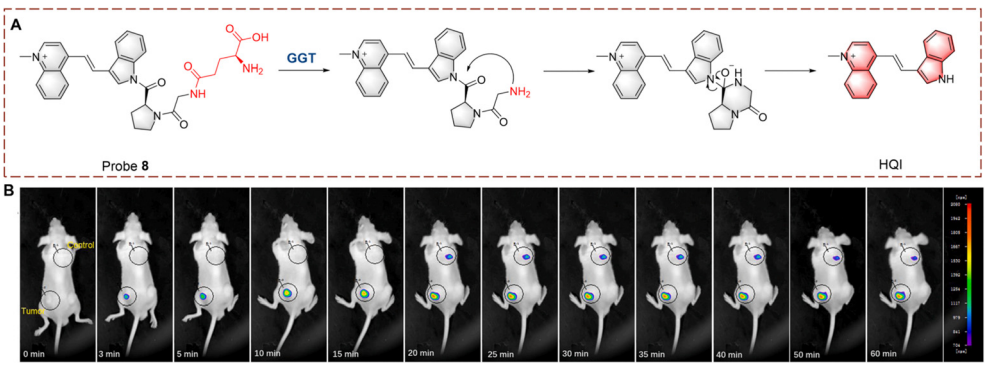

Fig. 8 (A) The structure and response mechanism of probe **8**. (B) Image of probe **8** in tumour-bearing mice (reprinted with permission from ref. 33 Copyright © 2022, Elsevier).

wavelength shift, which enables the ratiometric visualization of biocatalytic glutamine transfer.

Ahn *et al.* developed probe **9**, for monitoring GGT on cell membranes (Fig. 9).[34] The naphthalene ring acts as the fluorophore and the γ-glutamine acts as the recognition site. Probe **9** immobilizes in the cell membrane using a long-chain alkane and electrostatic interactions. When probe **9** is recognized, the γ-glutamine group is transferred, leading to the generation of an amino group. The product has stronger electron donating ability, resulting in fluorescence changes from green to red. Probe **9** was used the imaging of different cell lines and tissues using the wavelength change. In addition, the levels of GGT in cancer cells was found to be significantly higher than that for normal cells.

Kim *et al.* developed a ratiometric probe **10** for live cell imaging (Fig. 9).[35] Probe **10** was based on a benzothiazole attached to a naphthalene, to enhance the conjugation and fluorescence quantum yield. With γ-glutamine as a recognition group, probe **10** emits blue fluorescence. However, when probe **10** undergoes γ-glutamine transfer, the electron-donating amino group is released. This biocatalytic process changes the electron distribution of probe **10**, resulting in a red-shift of the wavelength (blue to green). In addition, oligoethylene glycol enhances the solubility of probe **10** in a physiological environment. Probe **10** exhibits excellent GGT selectivity and high fluorescence efficiency. Therefore, probe **10** could be used to quantitatively image GGT in human colon and cancer tissue.

Open Access Article. Published on 14 February 2024. Downloaded on 2/5/2026 3:32:46 PM.
This article is licensed under a Creative Commons Attribution 3.0 Unported Licence.

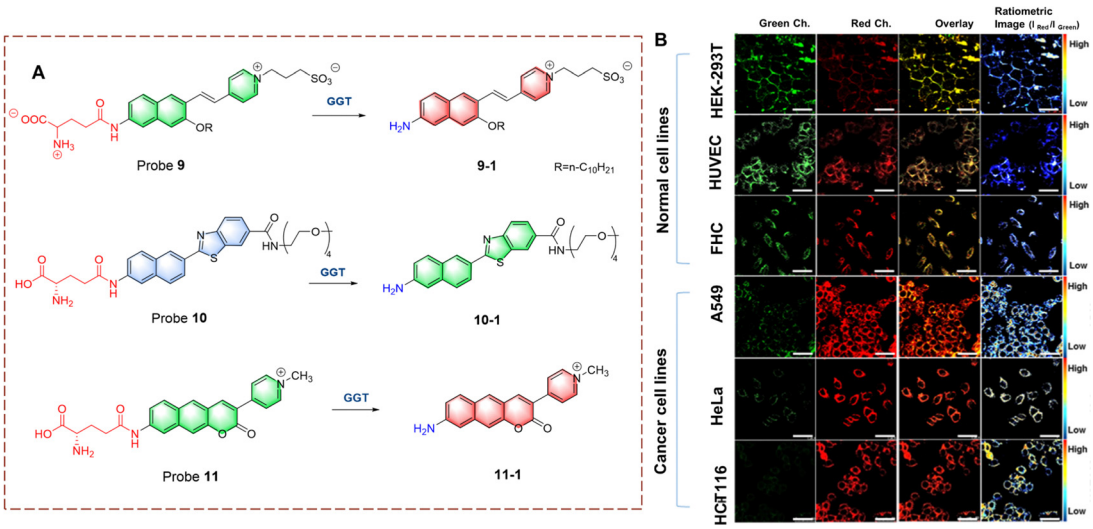

Fig. 9 (A) The structure and response mechanism of probe **9**, probe **10** and probe **11**. (B) Fluorescence images of normal cell lines and cancer cell lines with probe **9** (5.0 μM) (reprinted with permission from ref. 34 Copyright © 2020, American Chemical Society).

Ahn *et al.* have developed a ratiometric probe **11** which is not affected by environmental conditions (Fig. 9).[36] With benzo coumarin as the fluorophore, probe **11** emits green fluorescence. However, following transfer of the γ-glutamine group the wavelength is red-shifted (to red). Importantly, probe **11** is not affected by pH, viscosity and polarity changes, which solves problems associated with signal fluctuations. Therefore, probe **11** could be used for imaging HeLa cells and cancerous tissue. In addition, probe **11** exhibits potential as a quantitative analytic tool for complex biological systems.

Biocatalytic glucoside transfer

UDP-glucuronosyltransferases (UGTs) can catalyze the transfer of glucuronic acid to receptors under the conditions of UDP-glucuronic acid (UDPGA). This process plays an important role in the metabolic clearance of clinical drugs *in vivo*.[37–40] In addition, using glucosyltransferases (GTs) to achieve glycosylation has become an emerging method for industrial glycoside production.[41]

Ma *et al.* developed probe **12** for the real-time monitoring of glucoside transfer (Fig. 10).[42] The hemi cyanine acts as the fluorophore. To simultaneously preserve the fluorescence site of the hemi cyanine (6-OH) and the recognition site of UGT1A1 (5-OH), a "molecular splicing strategy" was used to synthesize probe **12**. Due to quenching by the *O*-diphenol, probe **12** was non-fluorescent. However, under biocatalysis by UGT1A1, the fluorescence is restored. Probe **12** is a highly selective near-infrared fluorescent probe. Therefore, probe **12** could be used for real-time UGT imaging of living cells and mice.

Ma *et al.* developed probe **13**, as a two-photon ratiometric fluorescent probe to detect GTs (Fig. 11).[43] The naphthalimide is used as the fluorophore, and the hydroxyl was used as the glycosylation site. Naphthalimide is a fluorescent group with high quantum yield, large Stokes shift, and good photostability, which is widely used in the field of fluorescence. In the presence of uridine diphosphate glucose (UDPG), a glucose group was transferred from UDPG to the phenolic hydroxyl group. After glycosylation the phenolic hydroxyl group is replaced by a glucose group, which causes a significant blue shift in the fluorescence of the glycosylation product (**13-1**). In addition, the fluorescence quantum yield of **13-1** is much higher than that of probe **13**, leading to an increase in fluorescence intensity. Using this platform, two fungi with glycosylation ability were successfully screened.

Using a similar strategy, James *et al.* developed probe **14** for screening GTs inhibitors for the prevention of dental caries (Fig. 11).[44] After biocatalytic glucosyl transfer the product (**14-1**) exhibits blue fluorescence emission, distinct from the yellow fluorescence of probe **14**. Probe **14** could be used for real-time

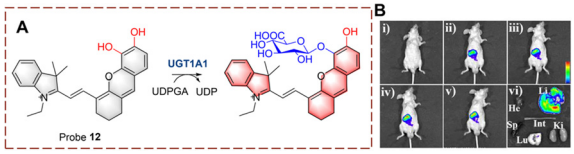

Fig. 10 (A) The structure and response mechanism of probe **12**. (B) Image of probe **12** (10 μM, 0–30 min) in mice and isolated organs (reprinted with permission from ref. 42 Copyright © 2021, John Wiley and Sons).

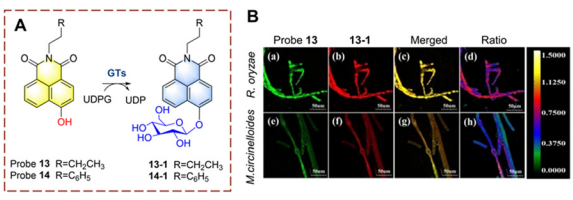

Fig. 11 (A) The structure and response mechanism of probe **13** and probe **14**. (B) Confocal microscopy images of probe **13** (50 μM, 8 h) and **13-1** in *R. oryzae* and *M. circinelloides* (reprinted with permission from ref. 43 Copyright © 2018, American Chemical Society).

This journal is © The Royal Society of Chemistry 2024

Open Access Article. Published on 14 February 2024. Downloaded on 2/5/2026 3:32:46 PM. This article is licensed under a Creative Commons Attribution 3.0 Unported Licence.

detection and imaging of GTs of cariogenic bacteria. In addition, inhibitors were screened from green tea for oral treatments.

Biocatalytic oxidation

Biocatalytic oxidation plays an important role in biological systems. The oxidation of glucose is the foundation of energy metabolism in organisms and an important pathway for obtaining energy. Carbon dioxide and water produced by its biocatalytic oxidation play a crucial role in maintaining the homeostasis of organisms. In addition, tyrosinase (TYR) directly affects the synthesis of melanin and participates in various physiological functions in the body, especially those involving antioxidants. The oxidation of monoamine substances in living organisms relies on MAOs. Research has found that mental illnesses such as depression, Parkinson's syndrome, and Alzheimer's disease are closely related to the activity of MAOs. Therefore, visual monitoring of the biocatalytic oxidation process is of great significance for the study of organisms and disease treatment.

Biocatalytic glucose oxidation

Many methods for detecting glucose biocatalytic oxidation use the H_2O_2 monitoring strategy. Detecting the H_2O_2 released during the oxidation process of glucose using glucose oxidase (GOD) can be used to monitor the biocatalytic process.[45] In addition sensors using carbon dots (CDs) and quantum dots (QDs) have been widely developed due to their advantages of simple operation and easy signal acquisition.[46–48] Liu *et al.* have developed a sensor DEMBs, consisting of two parts: rhodamine-modified silica microbeads (MBs) and CdTe (QDs) (Fig. 12).[49] MBs is the core and the QDs are the signal unit. When glucose is oxidized by oxidases, H_2O_2 is produced to quench the red fluorescence of the CdTe, while the green fluorescence of the rhodamine remains unchanged. When the biocatalytic reaction occurs, the **DEMBs** exhibit a specific red to green change in the fluorescence ratio. In addition, a colour change can be observed using naked eyes. As such, **DEMBs** have been used for the detection of glucose in serum. Significantly,

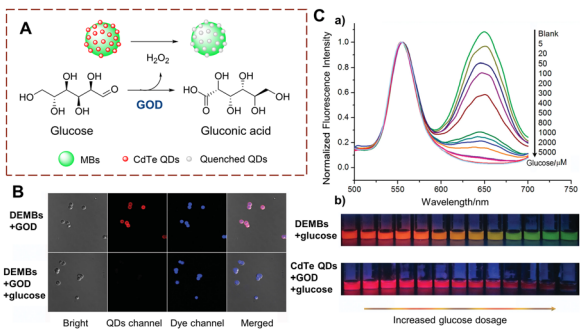

Fig. 12 (A) The structure and response mechanism of **DEMBs**. (B) Confocal images of **DEMBs** (6 mg mL^{-1}). (C) (a) Normalized fluorescence emission spectra of **DEMBs** (with GOD) treated with different concentrations of glucose; (b) confocal images of **DEMBs** and CdTe QDs treated with different concentrations of glucose (reprinted with permission from ref. 49 Copyright © 2016, John Wiley and Sons).

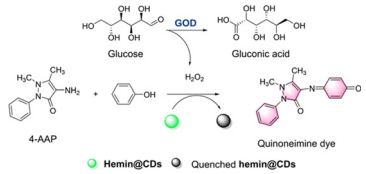

Fig. 13 The response mechanism of **hemin@CDs** (reprinted with permission from ref. 50 Copyright ©, 2020, Springer Nature).

these **DEMBs** can be used as general fluorescent sensors to detect any biocatalytic process that can produce H_2O_2.

Zhang *et al.* have developed a colorimetric fluorescent probe **hemin@CDs** (Fig. 13).[50] The CDs act as the probes for biocatalytic glucose oxidation by-product hydrogen peroxide. Meanwhile, the CDs support reduces the aggregation of hemin in the aqueous phase. In the presence of 4-aminoantipyrine (4-AAP), phenol and H_2O_2, the **hemin@CDs** catalyses a coupling reaction to produce a pink compound. **Hemin@CDs** exhibits the advantages of low-cost, rapid detection, and low detection limit. **Hemin@CDs** was successfully used to detect glucose and xanthine.

Biocatalytic tyrosine oxidation

Gold nanoclusters (AuNCs) have the advantages of resistance to photobleaching, good biocompatibility and easy handling. Therefore, they represent an excellent material for developing fluorescent sensors. Lu *et al.* developed a detection strategy using **AuNCs** to monitor TYR (Fig. 14).[51] After biocatalytic oxidation of tyrosine, a quinone is produced, and a cross-linking reaction forms melanoid oligomers. The oligomers continue to form a polymer spontaneously on the surface of **AuNCs**. The melanin-like polymer can quench the fluorescence of the **AuNCs**. However, this quenching can be significantly inhibited by H_2O_2. This method has the advantages of high selectivity and simplicity. As such the **AuNCs** can be used to detect cholesterol and acetylcholine sensitively.

QDs are also used for the detection of TYR.[52–55] Using antibody linked TYR, Ma *et al.* developed dopamine functionalized **DAs-QDs** that indirectly measures alpha-fetoprotein (AFP) (Fig. 15).[56] The sensor **DAs-QDs** is composed of CdSe/ZnS QDs and *N*-(3,4-dihydroxyphenethyl)-2-mercaptopentanamide (DAs). With AFP, the *ortho*-dihydroxyl group of the DAs is oxidized to

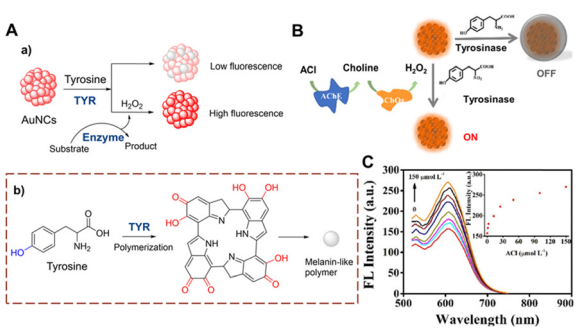

Fig. 14 (A) The response mechanism of **AuNCs** (a) and the generation of melanin-like polymer (b). (B) The illustration of **AuNCs** for ACl. (C) The fluorescence intensity spectra of **AuNCs** with different concentrations of ACl (0–150 μmol L^{-1}) (reprinted with permission from ref. 51 Copyright © 2019, Elsevier).

Open Access Article. Published on 14 February 2024. Downloaded on 2/5/2026 3:32:46 PM.
This article is licensed under a Creative Commons Attribution 3.0 Unported Licence.

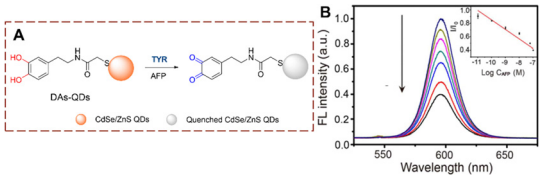

Fig. 15 (A) The structure and response mechanism of **DAs-QDs**. (B) The fluorescence intensity spectra of **DAs-QDs** to different concentrations of AFP (0–100 nM) (reprinted with permission from ref. 56 Copyright © 2016, American Chemical Society).

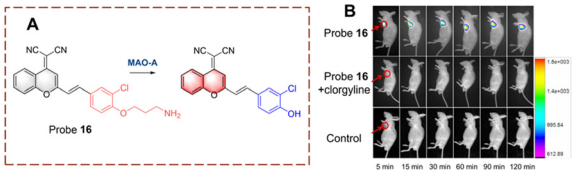

Fig. 17 (A) The structure and response mechanism of probe **16**. (B) Fluorescence images of probe **16** in tumour-bearing mice (reprinted with permission from ref. 63 Copyright © 2019, Royal Society of Chemistry).

quinones on the surface of the QDs. The quinone acts as an electron acceptor which can quench the QDs fluorescence. This fluorescence detection strategy exhibits low detection limit (10 pm), while being fast and simple. It provides an efficient method for AFP detection, which has the potential for clinical applications.

Biocatalytic monoamine oxidation

In the human body, biocatalytic oxidation of dopamine and phenethylamine is the primary mode of amine metabolism. MAO-A and MAO-B play key roles in this biocatalytic process.[57] Unfortunately, aberrant expression of MAOs damages nerve cells, which induces Parkinson's disease, Alzheimer's disease, depression and cancer.[58–61] Therefore, the development of visual methods to detect MAOs is of significance for the clinical diagnosis and treatment of neurological diseases.

Clorgyline as an inhibitor of MAO-A, has been widely used in the clinic. Thus, probes based on clorgyline have become useful molecular tools exhibiting the dual function of visualization and treatment.

Ma *et al.* have developed probe **15** by introducing a clorgyline segment into a hemi cyanine (Fig. 16).[62] To increase the flexibility of probe **15**, *N*,*N*′-dimethyl-1,2-ethanediamine carbamate has been introduced between the clorgyline segment and the hemi cyanine. When probe **15** is biocatalyzed, the amino is oxidatively removed. Subsequently, the *N*,*N*′-dimethyl-1,2-ethylenediamine carbamate acts as a self-immolating linker and dissociates from probe **15**, exposing the hydroxyl. ICT is recovered and the fluorophore is released. Probe **15** is a near-infrared fluorescence probe with high selectivity and sensitivity (LOD = 4.5 ng mL^{-1}). As such, probe **15** can be used for MAO-A imaging in cells, zebrafish and mice.

Using a similar strategy, Qin *et al.* have developed probe **16** (Fig. 17).[63] The dicyanomethylene (DCM) acts as the fluorophore which is linked to clorgyline through the C=C bond. Since the propylamine is attached to the hydroxyl, the ICT process is inhibited, resulting in the quenched fluorescence of probe **16**. When probe **16** is catalytically oxidized, the propylamine is removed and the phenolic hydroxyl group is recovered. Which results in a "D–π–A" structure that emits strong fluorescence. Probe **16** has the advantages of high selectivity, low detection limits (2.6 ng mL^{-1}), and rapid response (60 min).

Qin *et al.* developed a series of probes and using a screening approach determined that probe **17** was suitable for biocatalytic monoamine oxidation detection *in vivo* (Fig. 18).[64] Probe **17** is based on a dihydroxanthene (DH) which is linked to a 1,2,3,3-tetramethyl-3*H*-indol-1-ium. Probe **17** exhibits weak fluorescence, since the ICT process is inhibited by a propylamine which is attached to the hydroxyl. When the propylamine is catalytically oxidized, a carbonyl group is generated, followed by a β-elimination which exposes the hydroxyl on the anthracene and the fluorescence recovers due to ICT from the hydroxyl. Thus, probe **17** is suitable for monitoring biocatalytic oxidation by MAO-A. In addition, probe **17** was used for real-time detection of monoamine oxidation in mouse liver fibrosis tissue.

Ma *et al.* developed probe **18** for visualizing biocatalytic monoamine oxidation in living cells (Fig. 19).[65] The hemi cyanine hybrid coumarin acts as the fluorophore and propylamine acts as the recognition group. Probe **18** is non-fluorescent because propylamine is linked to the hydroxyl group of coumarin inhibiting ICT. When probe **18** undergoes biocatalysis, the amino group is oxidized to a carbonyl group, and subsequently, elimination

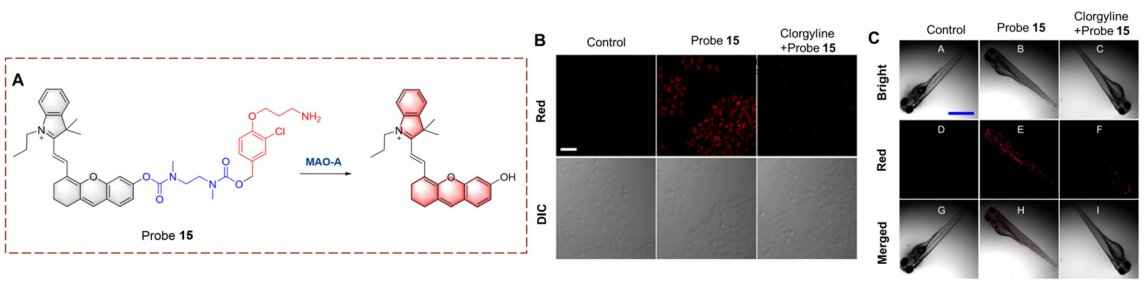

Fig. 16 (A) The structure and response mechanism of probe **15**. (B) Fluorescence images and the differential interference contrast (DIC) images of probe **15** (5 μM, 1 h) in HeLa cells. (C) Fluorescence images of probe **15** (5 μM, 1 h) in zebrafish (reprinted with permission from ref. 62 Copyright © 2021, American Chemical Society).

This journal is © The Royal Society of Chemistry 2024

Open Access Article. Published on 14 February 2024. Downloaded on 2/5/2026 3:32:46 PM.
This article is licensed under a Creative Commons Attribution 3.0 Unported Licence.

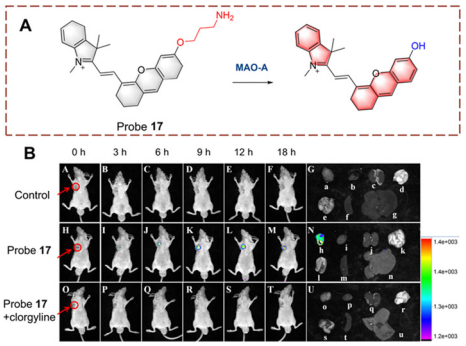

Fig. 18 (A) The structure and response mechanism of probe **17**. (B) Fluorescence images of probe **17** (50 μM) in SH-SY5Y tumour-bearing mice and isolated organs (reprinted with permission from ref. 64 Copyright © 2022, American Chemical Society).

occurs resulting in release of the coumarin hydroxyl. Thus, due to the recovery of the ICT process, probe **18** exhibits enhanced fluorescence in the mitochondria. Probe **18** was used as an effective strategy for the development of MAO-A inhibitors.

Tang *et al.* developed probe **19** for the rapid detection of biocatalytic amine oxidation (Fig. 20).[66] When probe **19** is oxidized, the amino is converted to an aldehyde group. Then, the aldehyde group reacts with the amino on the adjacent benzene to form a C═N bond. This reaction enhances the degree of conjugation in the system, resulting in strong fluorescence. Probe **19** has the remarkable advantages of simple preparation, fast detection (<10 min) and low detection limit (0.02 ng μL^{-1}). In addition, probe **19** was used for *in situ* imaging of deep tissue in mice with liver fibrosis, making it suitable for early diagnostic applications.

Biocatalytic reduction

Since cancer cells need to consume a large amount of oxygen for proliferation, hypoxia has become one of the main characteristics of the tumour microenvironment (TME).[67–70] Hypoxic conditions cause reductases such as nitroreductase (NTR) and azoreductase (AzoR) to be overexpressed in cancer cells.[71–76] Thus, the visual monitoring of biocatalytic nitro and azo-reductions are important for cancer diagnosis and treatment.

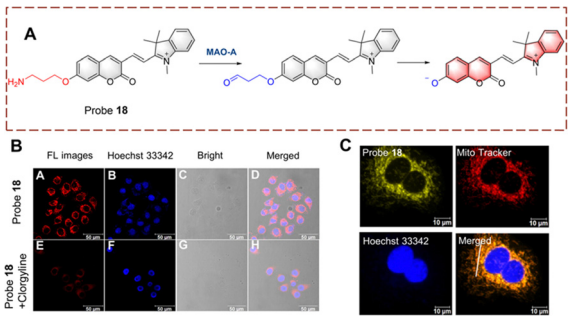

Fig. 19 (A) The structure and response mechanism of probe **18**. (B) Image of probe **18** in HeLa cells. (C) Mitochondrial localization imaging of probe **18** in HeLa cells (reprinted with permission from ref. 65 Copyright © 2022, Elsevier).

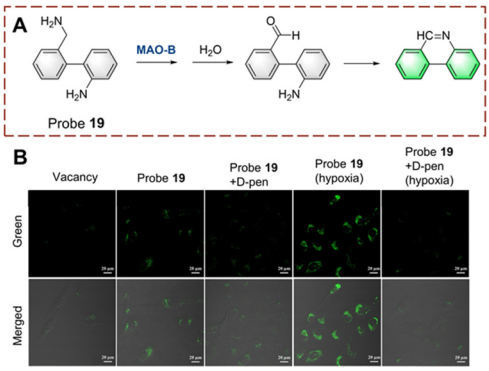

Fig. 20 (A) The structure and response mechanism of probe **19**. (B) Fluorescence images of probe **19** or probe **19** with D-pen (inhibitor) in LX-2 cells (reprinted with permission from ref. 66 Copyright © 2021, American Chemical Society).

Biocatalytic nitro reduction

Probes for monitoring biocatalytic nitro reduction have been developed with nitro as the recognition group and cyanine, naphthalimide, rhodamine and Nile-red as the fluorophores. Under the biocatalysis of NTR, the nitro group is recognized and reduced to an amino group. Due to this transformation from electron acceptor to donor, the fluorescence of the probe is turned on, enabling the visual detection of the biocatalytic nitro reduction.

Ge *et al.* have developed probe **20** with dual targeting of the mitochondria and lysosomes (Fig. 21).[77] With probe **20**, a benzo[*e*]indol aromatic azonia skeleton cyanine acted as the fluorophore, and nitrofuran acts as the recognition group. Significantly, the benzo[*e*]indol cation not only has the ability to target the mitochondria, but also can enhance the fluorescence intensity. The fluorescence of probe **20** is quenched due to the presence of the nitro group. Probe **20** exhibits good selectivity, fast response (180 s) and high sensitivity (LOD = 3.2 ng mL^{-1}). Therefore, probe **20** could be used to image HeLa cells. Additionally, the probe exhibited dual-targeting and could be used to detect NTR in the mitochondria and lysosomes.

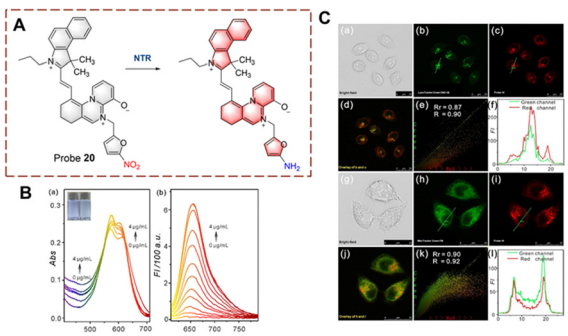

Fig. 21 (A) The structure and response mechanism of probe **20**. (B) The absorbance spectra (a) and fluorescent spectra (b) of probe **20**. (C) Confocal fluorescence images of probe **20**, LysoTracker Green DND-26 or Mito Tracker Green FM in HeLa cells (reprinted with permission from ref. 77 Copyright © 2020, Elsevier).

Open Access Article. Published on 14 February 2024. Downloaded on 2/5/2026 3:32:46 PM.
This article is licensed under a Creative Commons Attribution 3.0 Unported Licence.

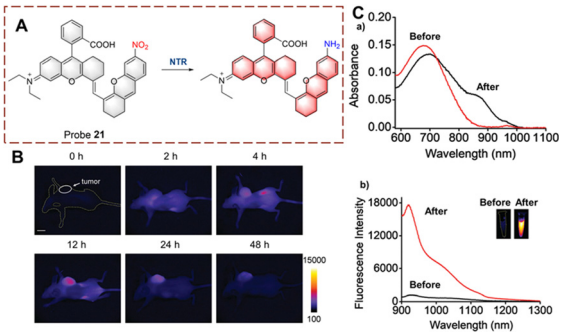

Fig. 22 (A) The structure and response mechanism of probe **21**. (B) Images of probe **21** in A549 tumour-bearing mice. (C) The absorbance spectra (a) and fluorescent spectra (b) of probe **21** before and after reduction (reprinted with permission from ref. 78 Copyright © 2021, Royal Society of Chemistry).

Ma *et al.* developed probe **21** for imaging the biocatalytic nitro reduction in the second near-infrared window (NIR-II) (Fig. 22).[78] Compared to NIR-I based probes, NIR-II based probes exhibit higher signal-to-noise ratio and deeper tissue penetration. Probe **21** is based on rhodamine hybrid polymethine. Initially, probe **21** exhibits no fluorescence due to the quenching effect of the nitro group. When the nitro group is catalytically reduced to an amino group, the fluorescence of probe **21** is recovered. Compared with other NIR-II probes, probe **21** displays a very low detection limit (3.2 ng mL^{-1}). Therefore, probe **21** could be used for tumour imaging *in vivo* due to its excellent deep tissue penetration.

NTR has become a common marker for hypoxia in living cells.[79,80] In addition, a decrease in intracellular oxygen can lead to changes in adenosine triphosphate (ATP).[81] Therefore, ATP is expected to become a marker that, together with NTR, illustrates the hypoxic state of cells. Based on this strategy, Ma *et al.* developed probe **22** for the simultaneous detection of NTR and ATP as markers for cellular hypoxia (Fig. 23).[82] Probe **22** was designed based on the rhodamine/1,8-naphthalimide

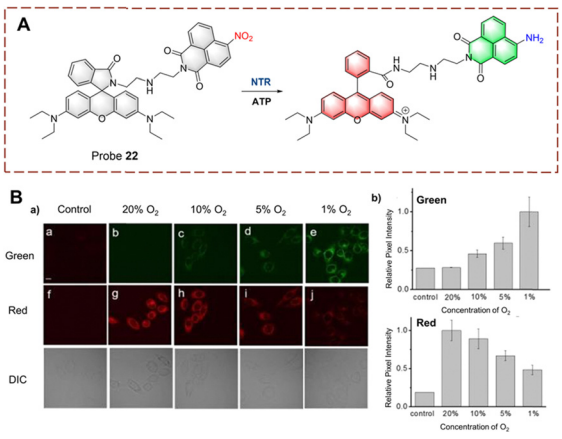

Fig. 23 (A) The structure and response mechanism of probe **22**. (B) Confocal fluorescence images of probe **22** in HeLa cells (a); relative pixel intensity of green channel and red channel (b) (reprinted with permission from ref. 82 Copyright © 2018, Royal Society of Chemistry).

hybrid structure. Diethylenetriamine and the nitro are the recognition elements for ATP and NTR, respectively. Due to the quenching effect of the nitro group and the formation of the spiroxamine, probe **22** exhibits weak fluorescence. However, when probe **22** is reduced, the nitro group is converted to an amine group. Moreover, in the presence of ATP, the spirolactam ring can be opened and probe **22** exhibits strong fluorescence. As a dual-function probe for the detection of NTR and ATP, probe **22** was used for anoxic cell imaging. Due to the synergistic effect of NTR and ATP, probe **22** is a more accurate tool for assessing hypoxia.

Hong *et al.* developed probe **23** for imaging in hypoxic mice (Fig. 24).[83] The system consists of a BF_2-chelated azadipyrromethane (BODIPY) as the fluorophore, and is linked to a *p*-nitrobenzyl group which can responded to NTR. The fluorescence is quenched due to the electron withdrawing effect of the *p*-nitrobenzyl group. When probe **23** undergoes reduction, the nitro group is converted to an electron-donating amino group. Then a 1,6-rearrangement elimination reaction occurs which results in the cleavage of the ether bond. The *p*-nitrobenzyl group is cleaved and the fluorophore is released, resulting in recovery of the fluorescence. Probe **23** exhibits the advantages of high sensitivity (LOD = 1.5 ng mL^{-1}) and rapid response (<5 min). Therefore, probe **23** could be used for tumour imaging *in vitro* and *in vivo*. Furthermore, probe **23** has the potential to be used in preoperative diagnosis of tumours.

Peng *et al.* developed a two-photon (TP) probe **24** for bioimaging the biocatalytic nitro reduction in mice (Fig. 25).[84] Probe **24** is a Nile-red derivative, and such fluorophores have previously been used as the TP fluorophore for other targets. TP fluorophores have the advantages of deep tissue penetration, lower background interference, and lower phototoxicity. With probe **24**, the *p*-nitrobenzyl group and the fluorophore are connected by an ether bond. When probe **24** undergoes a biocatalytic nitro reduction reaction, the nitro group is reduced to an amino group, and a 1,6-rearrangement elimination reaction occurs, which results in release of the Nile-red fluorophore. Probe **24** exhibits a 45-fold fluorescence enhancement at 655 nm. Additionally, probe **24** was used to image mouse liver sections and for *in vivo* imaging due to its deep tissue penetrating ability.

Based on the same mechanism, the Chen group developed probe **25** containing a hemi cyanine (Fig. 26).[85] Probe **25** exhibits weak fluorescence due to the quenching effect of the *p*-nitrophenzyl group. When probe **25** participates in the biocatalytic reduction reaction, the nitro group is reduced to an amino group, this is followed by a 1,6-rearrangement elimination reaction. Probe **25** is characterized by simple synthesis, high yield, wide detection range (0–20 μg mL^{-1}) and low detection limit (26 ng mL^{-1}). Based on these advantages, probe **25** was used to detect NTR in cells and mice under hypoxic conditions. Significantly, probe **25** was used for monitoring NTR under hyperbaric oxygen (HBO) treatment. As such the authors believe that probe **25** will become a pre-evaluation tool for surgery.

Biocatalytic azo reduction

Using the azo group as the recognition group, probes for detecting biocatalytic azo reduction have been developed.[86,87]

 This journal is © The Royal Society of Chemistry 2024

Open Access Article. Published on 14 February 2024. Downloaded on 2/5/2026 3:32:46 PM.
This article is licensed under a Creative Commons Attribution 3.0 Unported Licence.

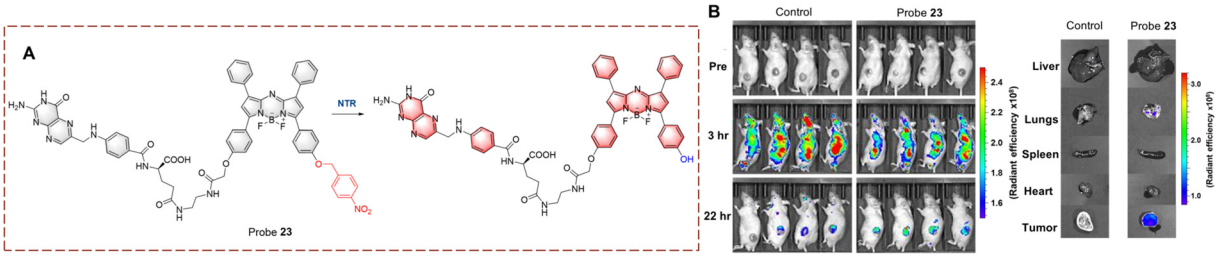

Fig. 24 (A) The structure and response mechanism of probe **23**. (B) Images of probe **23** in CT26 tumour-bearing mice and isolated organs (reprinted with permission from ref. 83 Copyright © 2021, American Chemical Society).

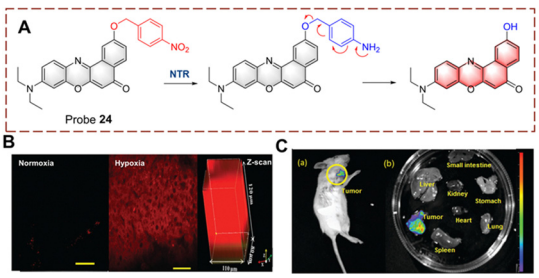

Fig. 25 (A) The structure and response mechanism of probe **24**. (B) TP imaging and confocal Z-scan images of probe **24** in mouse liver slices. (C) Fluorescence imaging of probe **24** in 4T1 tumour-bearing mice (a) and isolated organs (b) (reprinted with permission from ref. 84 Copyright © 2019, Royal Society of Chemistry).

The azo group can quench the fluorescence of a fluorophore, however, when the probe is reduced by a biocatalyst AzoR, the azo group is transformed into an electron donating amino group. As such this biocatalytic reaction results in a significant increase in the fluorescence of the probe.

Li developed probe **26** for monitoring biocatalytic azo reduction *in vivo* (Fig. 27).[88] A hemi cyanine acts as the fluorophore, and the azo group acts as both the recognition site and the quenching group. When probe **26** is reduced, the azo group is cleaved and an amino group is generated. The ICT process from amino to hemi-cyanine is then enabled resulting in fluorescence enhancement. Specifically, probe **26** is a NIR probe exhibiting high fluorescence enhancement (17-fold), high sensitivity (LOD = 0.017 μg mL^{-1}) and low biotoxicity. Therefore, probe **26** was used to monitor AzoR in mice with acute and chronic ulcerative colitis (UC). In addition, probe **26** was the first probe able to visualize changes of AzoR *in vivo*.

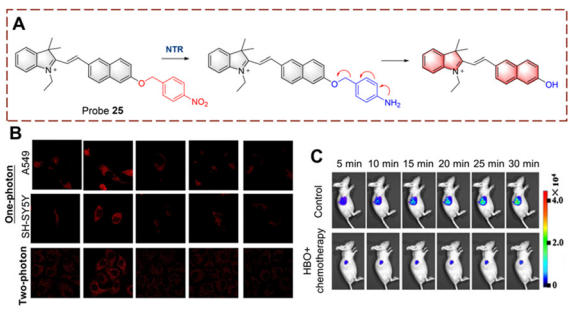

Fig. 26 (A) The structure and response mechanism of probe **25**. (B) Confocal microscopic images of probe **25** in SH-SY5Y cells and A549 cells during tumour treatment. (C) Image of probe **25** in A549 tumour-bearing mice (reprinted with permission from ref. 85 Copyright © 2020, Elsevier).

Biocatalytic hydrolysis

Hydrolases are biocatalytic enzymes found in living organisms that can accelerate the hydrolysis of large molecules into small molecules. They play an important role in the metabolism and decomposition processes of organisms. For example, small molecules are more easily absorbed and transformed by organisms, and metabolic waste can also be hydrolyzed and more easily excreted to maintain cellular balance.

Biocatalytic galactoside hydrolysis

β-Galactosidase is a hydrolase that catalyzes the hydrolysis of β-D-galactosides thus releasing terminal β-D-galactose units. This biocatalytic process is involved in cellular senescence and ovarian cancer.[89,90] Therefore, visual monitoring of biocatalytic galactoside hydrolysis is important to uncover its role in disease development. Probes are usually constructed containing a β-D-galactopyranoside and an appropriate fluorophore (*i.e.* naphthalimide, cyanine, and coumarin) for visual detection. The β-D-galactopyranoside is the recognition group linked to the fluorophore as a β-D-galactoside. Then under the biocatalytic action of β-galactosidase (β-Gal), the glycosidic group is cleaved, and the fluorophore is released with enhanced fluorescence.

Lin developed a ratiometric probe **27** for the detection of biocatalytic glycoside hydrolysis in cancer cells (Fig. 28).[91] Probe **27** uses a fluorescence resonance energy transfer (FRET) mechanism, with 7-diethylaminocoumarin and 4-hydroxy-1,8-naphthalimide as the donor (D) and acceptor (A). β-D-Galactopyranoside acts as a recognition group attached to the hydroxyl group of the naphthalimide, which results in reduced ICT and FRET. In this case, the blue fluorescence of probe **27** is from the coumarin. When probe **27** is hydrolyzed, the glycosidic bond is broken, and the hydroxyl group is released. The ICT process from the hydroxyl to naphthalimide is enabled, and the fluorescence is enhanced. While the absorption of the naphthalimide is red-shifted due to ICT, and FRET occurs with the coumarin, and probe **27** emits yellow fluorescence. Probe **27** is characterized by fast response (<20 s), high sensitivity

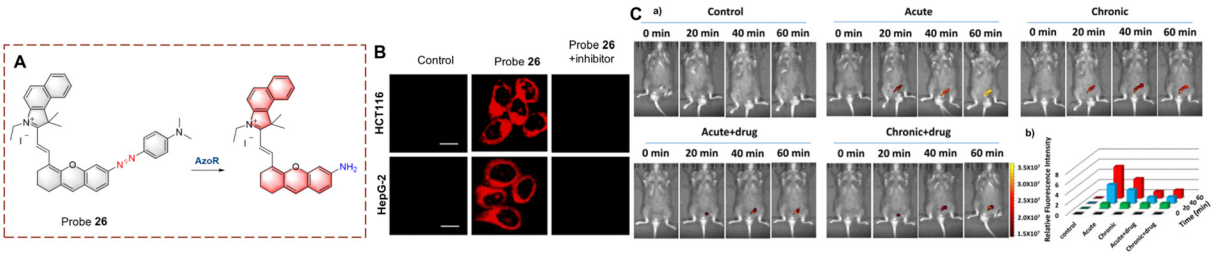

Fig. 27 (A) The structure and response mechanism of probe **26**. (B) Fluorescence imaging of probe **26** in HCT116 cells and HepG-2 cells. (C) (a) Fluorescence imaging of probe **26** in mice; (b) relative fluorescent intensity of (a) (reprinted with permission from ref. 88 Copyright © 2019, American Chemical Society).

Open Access Article. Published on 14 February 2024. Downloaded on 2/5/2026 3:32:46 PM.
This article is licensed under a Creative Commons Attribution 3.0 Unported Licence.

(LOD = 0.081 U mL^{-1}), high biocatalytic efficiency and good biocompatibility. As such, probe **27** was used to image live ovarian cancer cells (OVCAR-3 cells).

Liu *et al.* have developed probe **28** which exhibits lysosomal targeting (Fig. 29).[92] Probe **28** is based on a hemi cyanine fluorophore, with β-D-galactopyranoside recognition group. The lysosome-targeting ability of probe **28** is due to the morpholine group. Initially, probe **28** is non-fluorescent because the hydroxyl group is caged by the β-D-galactopyranoside. When probe **28** targets the lysosome to participate in biocatalytic processes, the β-D-galactopyranoside is then cleaved. Resulting in the production of a phenolate intermediate which undergoes a 1,6-elimination reaction. As such, probe **28** emits strong fluorescence due to the recovery of the ICT process. Since probe **28** exhibits rapid response (<1 min). it could be used for the visual detection of endogenous β-Gal in ovarian cancer cells.

Zhu *et al.* developed a ratiometric probe **29** for monitoring biocatalytic galactoside hydrolysis (Fig. 30).[93] Probe **29** is based on BODIPY and the hydroxyl group is conjugated through a C=C bond. This conjugated system has been shown to have a remarkable ICT effect. In probe **29**, β-D-galactopyranoside is used as the recognition group masking the hydroxyl group. When probe **29** is catalytically hydrolyzed, the β-D-galactopyranoside is cleaved and converted to the phenolate intermediate. As a result, the hydroxyl group is exposed, and the ICT process is turned on with a significant red shift (575 nm to 730 nm). During the hydrolysis of probe **29**, a shift in the absorption peak from 560 nm to 620 nm occurs resulting in a colour change from pink to dark blue. Making it possible to observe the activity of the β-Gal using naked eyes.

Guo *et al.* has extracted hyperoside from *Hedyotis diffusa* as a probe **30** (Fig. 31).[94] The β-galactoside is hydrolyzed and cleaved after being recognized by β-Gal. Subsequently, the hydrolyzed product quercetin was released and aggregates *in situ*. Quercetin was shown to be an aggregation-induced emission luminophore (AIEgen) with excited-state intramolecular proton transfer (ESIPT) properties.[95,96] The C=O and hydroxyl in quercetin act as proton acceptor and donor respectively, so intramolecular hydrogen bonds are easily formed. However, probe **30** does not exhibit aggregative luminescence since the hydroxyl group is caged by the β-galactoside. Probe **30** is a natural substance that is easy to obtain and exhibits the advantages of high selectivity, high sensitivity (0.013 U mL^{-1}), long-term imaging (8 h) and low toxicity. As such, probe **30** has been used to perform transient and long-term imaging in human ovarian cancer cells.

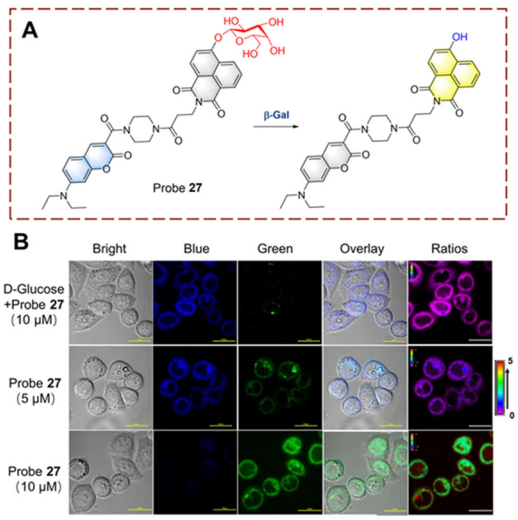

Fig. 28 (A) The structure and response mechanism of probe **27**. (B) Fluorescent imaging of probe **27** in OVCAR-3 cells (reprinted with ref. 91 Copyright © 2019, American Chemical Society).

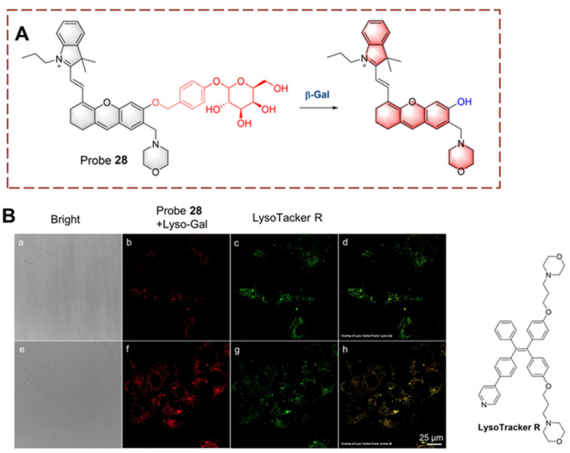

Fig. 29 (A) The structure and response mechanism of probe **28**. (B) Fluorescence images of probe **28** or LysoTracker R in SKOV-3 cells (reprinted with ref. 92 Copyright © 2020, American Chemical Society).

This journal is © The Royal Society of Chemistry 2024

Open Access Article. Published on 14 February 2024. Downloaded on 2/5/2026 3:32:46 PM.
This article is licensed under a Creative Commons Attribution 3.0 Unported Licence.

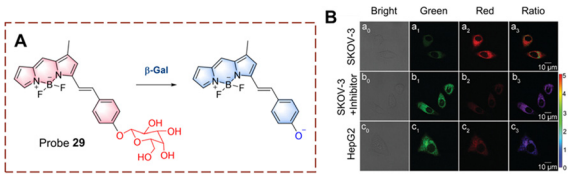

Fig. 30 (A) The structure and response mechanism of probe **29**. (B) Fluorescence images of probe **29** in SKOV-3 and HepG-2 cells (reprinted with permission from ref. 93 Copyright © 2019, Royal Society of Chemistry).

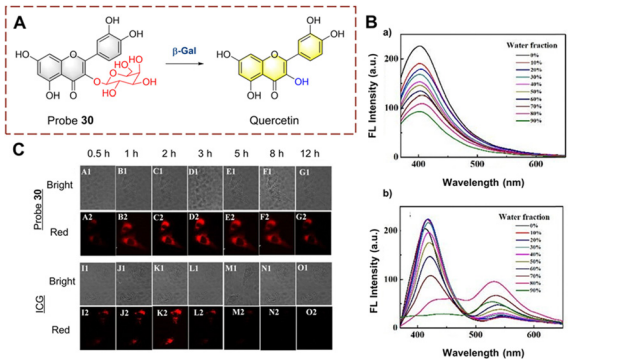

Fig. 31 (A) The structure and response mechanism of probe **30**. (B) The fluorescence intensity spectra of probe **30** (a) and quercetin (b) (THF/H_2O). (C) Images of probe **30** and ICG in SKOV-3 cells (reprinted with permission from ref. 94 Copyright © 2020, Royal Society of Chemistry).

Biocatalytic phosphate hydrolysis

In humans, the biocatalytic hydrolysis of phosphate groups in proteins is of great significance for disease diagnosis. This biocatalytic process relies on phosphatases.[97–99] Therefore, the visual detection of phosphate hydrolysis is significant for a full understanding of the mechanism of biocatalysts and improved treatment strategies.

Yao *et al.* have developed **YP4** for the detection and imaging of phosphatase activity (Fig. 32).[100] **YP4** is constructed using a two-photon fluorophore (**Y1**). The phosphate group acts as recognition group. While the phenol hydroxyl is caged by electron-withdrawing phosphate, resulting in the reduction of the conjugated π-electron system, thus **YP4** is non fluorescent. **YP4** consist of two units a fluorescent group connected to a cell penetrating peptide CPP with masking peptide attached. Initially **YP4** cannot enter cells but on cleavage of the masking peptide by matrix metalloproteases (MMPs), **YP4** can be absorbed into cells. After **YP4** enters the cell, and subsequent UV irradiation can remove the 2-nitrobenzyloxy, thus exposing the phosphate group. The phosphatase then removes the phosphate group and the fluorescence is restored. **YP4** exhibits good photophysical properties, deep tissue penetration (110 μm) and low background interference. Therefore, **YP4** has been used to image phosphatase in cancer cells and Drosophila cerebrum. Importantly, **YP4** exhibits two-photon photophysical properties for the detection of endogenous phosphatase activity.

Conclusions

Fluorescence techniques enable the visual monitoring of biocatalysis, which enables the understanding of catalytic mechanisms in biological systems. With this highlight we have outlined strategies for monitoring biocatalysts including (1) biocatalytic γ-glutamine transfer: linking a γ-glutamine to fluorophores including cyanine, coumarin and naphthalimide, quenches the fluorescence; then once the glutamine group is transferred, the amino group formed recovers the fluorescence. (2) Biocatalytic monoamine oxidation: attaching propylamine to fluorophores including cyanine and rhodamine, masks the hydroxyl and blocks ICT, after oxidation, a carbonyl group is produced with concomitant β-elimination of PABA facilitating the recovery of ICT and enhanced fluorescence. (3) Biocatalytic nitro reduction: linking a nitro group or *p*-nitrobenzyl group to fluorophores including cyanine, BODIPY, Nile-red and naphthalimide, the fluorescence is quenched. When the nitro group is reduced, the quenching effect is removed and fluorescence is recovered. (4) Biocatalytic β-galactoside hydrolysis: attaching a β-D-galactopyranoside to a fluorophore including BODIPY, coumarin-naphthalimide and natural quercetin, generates a masked hydroxyl group generating a ratiometric fluorescence system. Using these strategies, monitoring biological and pathological processes in cells or *in vivo* becomes

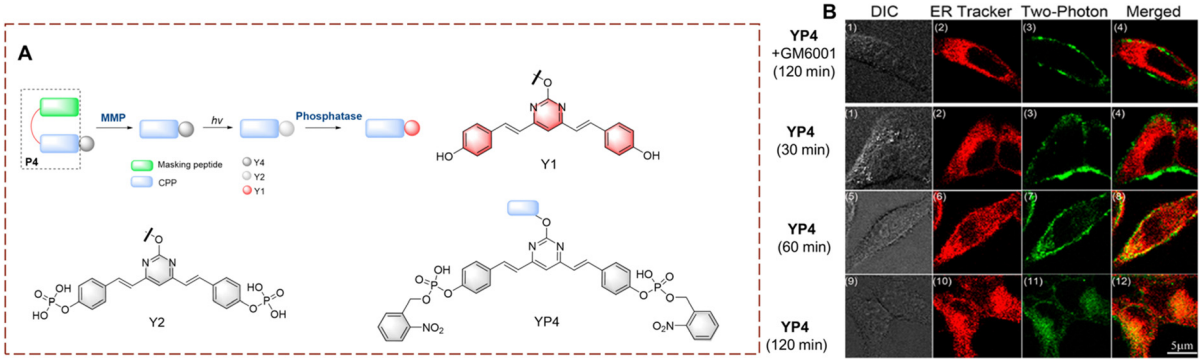

Fig. 32 (A) The structure and response mechanism of **YP4**, Y2 and Y1. (B) Two-photon fluorescence microscopy (TPFM) of **YP4** or **YP4** with GM6001 (MMP inhibitor) in HeLa cells (reprinted with permission from ref. 100 Copyright © 2012, American Chemical Society).

Open Access Article. Published on 14 February 2024. Downloaded on 2/5/2026 3:32:46 PM. This article is licensed under a Creative Commons Attribution 3.0 Unported Licence.

possible. We anticipate that in the future, biocatalytic probes will become ubiquitous in disease monitoring and treatment and help contribute to the rapid development and advancement of precision medicine.

Author contributions

Guang Chen, Jie Xu, Siyue Ma and Chao Wang wrote and edited the original draft. Xiaoyong Gao and Ji Chen contributed to the scientific illustrations in the manuscript. Xinrui Ji, Jared B. Carney and Pu Chen created an outline for the review paper. Tony D. James, Yanfeng Yue and Baolei Fan conceived the topic and revised the manuscript. All authors contributed to the final checking of the manuscript.

Conflicts of interest

TDJ acts as an academic consultant for Jiangsu Simba Biological Medicine Co., Ltd.

Acknowledgements

This work supported by the National Natural Science Foundation of China (22174090); the Natural Science Basic Research Program of Shaanxi (2022JM-089); Long-term Project of high-level talents innovation in Shaanxi Province (Guang Chen); XJ and PC wishes to thank the High-end project of National Foreign Expert Program (G2021041002L); SM thanks the fellowship of China Postdoctoral Science Foundation (2022M711994); Key R&D Program of Shaanxi Province (2022GY-203); Science and Technology Plan Project of Weiyang District (202114); Science and Technology Plan Project of Xi'an (21NYYF0057). TDJ wishes to thank the University of Bath and the Open Research Fund of the School of Chemistry and Chemical Engineering, Henan Normal University (2020ZD01) for support. BF wishes to thank the Key R&D Plan of Hubei Province for local special support in the field of general health (2022BCE066).

References

1 H. Yan, P. Xu, H. Ma, Y. Li, R. Zhang, H. Cong, B. Yu and Y. Shen, *Biomaterials*, 2023, **301**, 122213.
2 S. Yardim Akaydin, E. Miser Salihoglu, D. Gelen Gungor, H. Karanlik and S. Demokan, *Eur. J. Breast Health*, 2020, **16**, 72–76.
3 Y. Santin, J. Resta, A. Parini and J. Mialet-Perez, *Ageing Res. Rev.*, 2021, **66**, 101256.
4 S. Wang, X.-F. Zhang, H.-S. Wang, J. Liu, S.-L. Shen and X.-Q. Cao, *Talanta*, 2023, **252**, 123834.
5 Y. Wang, X. Han, X. Zhang, L. Zhang and L. Chen, *Analyst*, 2020, **145**, 1389–1395.
6 Z. Tang, Z. Yan, L. Gong, L. Zhang, X. Yin, J. Sun, K. Wu, W. Yang, G. Fan, Y. Li and H. Jiang, *Anal. Chem.*, 2022, **94**, 14778–14784.
7 Y. Kim, H. Li, J. Choi, J. Boo, H. Jo, J. Y. Hyun and I. Shin, *Chem. Soc. Rev.*, 2023, **52**, 7036–7070.
8 P. K. Hashim, H. M. Dokainish and N. Tamaoki, *Org. Biomol. Chem.*, 2023, **21**, 6120–6123.
9 B. Feng, F. Chu, X. Huang, Y. Fang, M. Liu, M. Liu, F. Chen and W. Zeng, *Sens. Actuators, B*, 2023, **396**, 134541.
10 G. Cabrera, T. Linares, M. E. de la Calle, D. Cantero, A. Valle and J. Bolivar, *Int. J. Mol. Sci.*, 2020, **21**, 8523.
11 K. Norvaisa, M. Kielmann and M. O. Senge, *ChemBioChem*, 2020, **21**, 1793–1807.
12 S. R. B. R. A. A. Husain, S. Chatterjee, I. Khan and Z. Lin, *J. Mater. Chem. B*, 2020, **8**, 3192–3212.
13 G. Kovacevic, R. Ostafe, A. M. Balaz, R. Fischer and R. Prodanovic, *J. Biosci. Bioeng.*, 2019, **127**, 30–37.
14 D. Ning, Q. Liu, Q. Wang, X.-M. Du, W.-J. Ruan and Y. Li, *Sens. Actuators, B*, 2019, **282**, 443–448.
15 H. Fang, H. Zhang, L. Li, Y. Ni, R. Shi, Z. Li, X. Yang, B. Ma, C. Zhang, Q. Wu, C. Yu, N. Yang, S. Q. Yao and W. Huang, *Angew. Chem., Int. Ed.*, 2020, **59**, 7536–7541.
16 S. Wu, R. Snajdrova, J. C. Moore, K. Baldenius and U. T. Bornscheuer, *Angew. Chem., Int. Ed.*, 2020, **60**, 88–119.
17 D. A. Holland-Moritz, M. K. Wismer, B. F. Mann, I. Farasat, P. Devine, E. D. Guetschow, I. Mangion, C. J. Welch, J. C. Moore, S. Sun and R. T. Kennedy, *Angew. Chem., Int. Ed.*, 2020, **59**, 4470–4477.
18 Q. Meng, C. Ramirez-Palacios, N. Capra, M. E. Hooghwinkel, S. Thallmair, H. J. Rozeboom, A. W. H. Thunnissen, H. J. Wijma, S. J. Marrink and D. B. Janssen, *ACS Catal.*, 2021, **11**, 10733–10747.
19 C. Wang, K. Tang, Y. Dai, H. Jia, Y. Li, Z. Gao and B. Wu, *ACS Omega*, 2021, **6**, 17058–17070.
20 F. Cheng, X. L. Chen, C. Xiang, Z. Q. Liu, Y. J. Wang and Y. G. Zheng, *Appl. Microbiol. Biotechnol.*, 2020, **104**, 2999–3009.
21 T. Scheidt, H. Land, M. Anderson, Y. Chen, P. Berglund, D. Yi and W.-D. Fessner, *Adv. Synth. Catal.*, 2015, **357**, 1721–1731.
22 K. Takemura, P. G. Board and F. Koga, *Antioxidants*, 2021, **10**, 549.
23 F. Liu, D. Zhu, Y. Li, M. Kong, Y. Li, J. Luo and L. Kong, *Sens. Actuators, B*, 2022, **363**, 131838.
24 Q. Liu, J. Yuan, R. Jiang, L. He, X. Yang, L. Yuan and D. Cheng, *Anal. Chem.*, 2023, **95**, 2062–2070.
25 R. Obara, M. Kamiya, Y. Tanaka, A. Abe, R. Kojima, T. Kawaguchi, M. Sugawara, A. Takahashi, T. Noda and Y. Urano, *Angew. Chem., Int. Ed.*, 2020, **60**, 2125–2129.
26 S. M. Usama, F. Inagaki, H. Kobayashi and M. J. Schnermann, *J. Am. Chem. Soc.*, 2021, **143**, 5674–5679.
27 N. He, Y. Wang, Y. Huang, X. Wang, L. Chen and C. Lv, *Sens. Actuators, B*, 2020, **322**, 128565.
28 F. Liu, Z. Wang, T. Zhu, W. Wang, B. Nie, J. Li, Y. Zhang, J. Luo and L. Kong, *Talanta*, 2019, **191**, 126–132.
29 H. Li, Q. Yao, F. Xu, N. Xu, R. Duan, S. Long, J. Fan, J. Du, J. Wang and X. Peng, *Biomaterials*, 2018, **179**, 1–14.
30 P. Siarkiewicz, R. Michalski, A. Sikora, R. Smulik-Izydorczyk, M. Szala, A. Grzelakowska, J. Modrzejewska, A. Bailey, J. E. Nycz, B. Kalyanaraman, J. G. Malecki, J. Zielonka and R. Podsiadły, *Dyes Pigm.*, 2021, **192**, 109405.
31 Y. Li, C. Xue, Z. Fang, W. Xu and H. Xie, *Anal. Chem.*, 2020, **92**, 15017–15024.
32 R. An, S. Wei, Z. Huang, F. Liu and D. Ye, *Anal. Chem.*, 2019, **91**, 13639–13646.
33 H. Xue, J. Lu, H. Yan, J. Huang, H. B. Luo, M. S. Wong, Y. Gao, X. Zhang and L. Guo, *Talanta*, 2022, **237**, 122898.
34 Y. J. Reo, M. Dai, Y. J. Yang and K. H. Ahn, *Anal. Chem.*, 2020, **92**, 12678–12685.
35 Y. J. Kim, S. J. Park, C. S. Lim, D. J. Lee, C. K. Noh, K. Lee, S. J. Shin and H. M. Kim, *Anal. Chem.*, 2019, **91**, 9246–9250.
36 Y. J. Reo, Y. W. Jun, S. Sarkar, M. Dai and K. H. Ahn, *Anal. Chem.*, 2019, **91**, 14101–14108.
37 Y.-B. Luo, Y.-Y. Hou, Z. Wang, X.-M. Hu, W. Li, Y. Li, Y. Liu, T.-J. Li and C.-Z. Ai, *Comput. Biol. Med.*, 2022, **149**, 105959.
38 X.-F. Zhai, Y. Yi, R. Yu, Y. Kuang, S. Shaker, H.-F. Su, G. Ye, C.-R. Liu, X. Qiao, L. Liang and M. Ye, *Sens. Actuators, B*, 2022, **364**, 131826.
39 Z. Tian, J. Wang, Y. Gao, X. Huo, Z. Yu, Y. Wang, C. Wang, L. Feng, J. Cui and X. Tian, *Sens. Actuators, B*, 2022, **369**, 132342.
40 X.-F. Zhai, J.-J. Fan, Y. Yi, M. Zhang, X. Yuan, X. Qiao, L. Liang and M. Ye, *Chem. Eng. J.*, 2023, **463**, 142382.
41 A. Andreu, M. Ćorović, C. Garcia-Sanz, A. S. Santos, A. Milivojević, C. Ortega-Nieto, C. Mateo, D. Bezbradica and J. M. Palomo, *Catalysts*, 2023, **13**, 1359.
42 X. Tian, T. Liu, Y. Ma, J. Gao, L. Feng, J. Cui, T. D. James and X. Ma, *Angew. Chem., Int. Ed.*, 2021, **60**, 24566–24572.
43 L. Feng, P. Li, J. Hou, Y. L. Cui, X. G. Tian, Z. L. Yu, J. N. Cui, C. Wang, X. K. Huo, J. Ning and X. C. Ma, *Anal. Chem.*, 2018, **90**, 13341–13347.
44 L. Feng, Q. Yan, B. Zhang, X. Tian, C. Wang, Z. Yu, J. Cui, D. Guo, X. Ma and T. D. James, *Chem. Commun.*, 2019, **55**, 3548–3551.

 This journal is © The Royal Society of Chemistry 2024

Open Access Article. Published on 14 February 2024. Downloaded on 2/5/2026 3:32:46 PM. This article is licensed under a Creative Commons Attribution 3.0 Unported Licence.

45 H. Zhao, X. Yuan, X. Yang, F. Bai, C. Mao and L. Zhao, *Inorg. Chem.*, 2021, **60**, 15485–15496.
46 X. Li, S. Zhao, B. Li, K. Yang, M. Lan and L. Zeng, *Coord. Chem. Rev.*, 2021, **431**, 213686.
47 C. Niu, Z. Yao and S. Jiang, *Sci. Total Environ.*, 2023, **882**, 163565.
48 Q. Yang, C. Li, J. Li, M. Arabi, X. Wang, H. Peng, H. Xiong, J. Choo and L. Chen, *J. Mater. Chem. C*, 2020, **8**, 5554–5561.
49 X. Lu, P. Wang, Y. Wang, C. Liu and Z. Li, *Adv. Mater. Technol.*, 2016, **1**, 1600024.
50 L. Su, Y. Cai, L. Wang, W. Dong, G. Mao, Y. Li, M. Zhao, Y. Ma and H. Zhang, *Mikrochim. Acta*, 2020, **187**, 132.
51 X. Yan, H. Li, R. Jin, X. Zhao, F. Liu and G. Lu, *Sens. Actuators, B*, 2019, **279**, 281–288.
52 X. Cheng, Y. Chai, J. Xu, L. Wang, F. Wei, G. Xu, Y. Sun, Q. Hu and Y. Cen, *Sens. Actuators, B*, 2020, **309**, 127765.
53 Y. Liu, Y. Zhang, X. Zhang, W. Zhang, X. Wang, Y. Sun, P. Ma, Y. Huang and D. Song, *Sens. Actuators, B*, 2021, **344**, 130234.
54 S. Li, R. Zhao, M. Ma, G. Fu, S. Mu, T. Han, X. Liu and H. Zhang, *Sens. Actuators, B*, 2022, **370**, 132438.
55 M. Wang, J.-L. Xie, J. Li, Y.-Y. Fan, X. Deng, H.-L. Duan and Z.-Q. Zhang, *ACS Sens.*, 2020, **5**, 1634–1640.
56 W. H. Zhang, W. Ma and Y. T. Long, *Anal. Chem.*, 2016, **88**, 5131–5136.
57 H. U. Cho, S. Kim, J. Sim, S. Yang, H. An, M. H. Nam, D. P. Jang and C. J. Lee, *Exp. Mol. Med.*, 2021, **53**, 1148–1158.
58 W. Y. Kim, M. Won, A. Salimi, A. Sharma, J. H. Lim, S.-H. Kwon, J.-Y. Jeon, J. Y. Lee and J. S. Kim, *Chem. Commun.*, 2019, **55**, 13267–13270.
59 Y. Shu, Y. Liu, Y. Gao and J. Li, *Sens. Actuators, B*, 2023, **390**, 133912.
60 H. Fang, H. Zhang, L. Li, Y. Ni, R. Shi, Z. Li, X. Yang, B. Ma, C. Zhang, Q. Wu, C. Yu, N. Yang, S. Q. Yao and W. Huang, *Angew. Chem.*, 2020, **132**, 7606–7611.
61 Y. Mei, Z. Liu, M. Liu, J. Gong, X. He, Q.-W. Zhang and Y. Tian, *Chem. Commun.*, 2022, **58**, 6657–6660.
62 J. Shang, W. Shi, X. Li and H. Ma, *Anal. Chem.*, 2021, **93**, 4285–4290.
63 Z. Yang, W. Li, H. Chen, Q. Mo, J. Li, S. Zhao, C. Hou, J. Qin and G. Su, *Chem. Commun.*, 2019, **55**, 2477–2480.
64 Z. M. Yang, Q. Y. Mo, J. M. He, D. L. Mo, J. Li, H. Chen, S. L. Zhao and J. K. Qin, *ACS Sens.*, 2020, **5**, 943–951.
65 J. Wu, C. Han, X. Cao, Z. Lv, C. Wang, X. Huo, L. Feng, B. Zhang, X. Tian and X. Ma, *Anal. Chim. Acta*, 2022, **1199**, 339573.
66 N. Fan, C. Wu, Y. Zhou, X. Wang, P. Li, Z. Liu and B. Tang, *Anal. Chem.*, 2021, **93**, 7110–7117.
67 L. Gai, Y. Liu, Z. Zhou, H. Lu and Z. Guo, *Coord. Chem. Rev.*, 2023, **481**, 215041.
68 K. Mortezaee and J. Majidpoor, *Life Sci.*, 2021, **286**, 120057.
69 R. C. Augustin, G. M. Delgoffe and Y. G. Najjar, *Cancers*, 2020, **12**, 3802.
70 A. Vito, N. El-Sayes and K. Mossman, *Cells*, 2020, **9**, 992.
71 S. Wang, W. Tan, W. Lang, H. Qian, S. Guo, L. Zhu and J. Ge, *Anal. Chem.*, 2022, **94**, 7272–7277.
72 J. Zhou, S. Fang, D. Zhang, Y. Qu, L. Wang, S. Pan, L. Li, J. Li, W. Du and Q. Wu, *Sens. Actuators, B*, 2023, **390**, 134015.
73 K.-C. Yan, J. E. Gardiner, A. C. Sedgwick, N. Thet, R. A. Heylen, T. D. James, A. T. A. Jenkins and X.-P. He, *Chem. Commun.*, 2023, **59**, 8278–8281.
74 L.-L. Wu, Q. Wang, Y. Wang, N. Zhang, Q. Zhang and H.-Y. Hu, *Chem. Sci.*, 2020, **11**, 3141–3145.
75 L. Fan, Q. Zan, B. Lin, X. Wang, X. Gong, Z. Zhao, S. Shuang, C. Dong and M. S. Wong, *Analyst*, 2020, **145**, 5657–5663.
76 L. Guo, P. Wang, H. Chen, X. Fan, H. L. Zhu and Z. Li, *Mater. Today Chem.*, 2022, **25**, 100928.
77 X.-L. Sha, X.-Z. Yang, X.-R. Wei, R. Sun, Y.-J. Xu and J.-F. Ge, *Sens. Actuators, B*, 2020, **307**, 127653.
78 X. Zhang, X. Li, W. Shi and H. Ma, *Chem. Commun.*, 2021, **57**, 8174–8177.
79 J. Yan, K. Wang, L. Gui, X. Liu, Y. Ji, J. Lin, M. Luo, H. Xu, J. Lv, F. Tan, L. Lin and Z. Yuan, *Anal. Chem.*, 2023, **95**, 14402–14412.
80 B. Hu, N. Song, Y. Cao, M. Li, X. Liu, Z. Zhou, L. Shi and Z. Yu, *J. Am. Chem. Soc.*, 2021, **143**, 13854–13864.
81 S. Chen, D. Yu, W. Zhong, J. Liu, J. Liu, B. Liu, J. Zheng and R. Yang, *Chem. Commun.*, 2021, **57**, 7786–7789.
82 Y. Fang, W. Shi, Y. Hu, X. Li and H. Ma, *Chem. Commun.*, 2018, **54**, 5454–5457.
83 S. Karan, M. Y. Cho, H. Lee, H. Lee, H. S. Park, M. Sundararajan, J. L. Sessler and K. S. Hong, *J. Med. Chem.*, 2021, **64**, 2971–2981.
84 K. H. Gebremedhin, Y. Li, Q. Yao, M. Xiao, F. Gao, J. Fan, J. Du, S. Long and X. Peng, *J. Mater. Chem. B*, 2019, **7**, 408–414.
85 Y. Wang, L. Zhang, Y. Huang, X. Wang, L. Zhang and L. Chen, *Sens. Actuators, B*, 2020, **310**, 127755.
86 Y. Tian, Y. Li, W.-X. Wang, W.-L. Jiang, J. Fei and C.-Y. Li, *Anal. Chem.*, 2020, **92**, 4244–4250.
87 X.-b Zhao, W. Ha, K. Gao and Y.-p Shi, *Anal. Chem.*, 2020, **92**, 9039–9047.
88 Y. Tian, Y. Li, W. L. Jiang, D. Y. Zhou, J. Fei and C. Y. Li, *Anal. Chem.*, 2019, **91**, 10901–10907.
89 Y. Gao, Y. Hu, Q. Liu, X. Li, X. Li, C. Y. Kim, T. D. James, J. Li, X. Chen and Y. Guo, *Angew. Chem., Int. Ed.*, 2021, **60**, 10756–10765.
90 Y. Yao, Y. Zhang, C. Yan, W.-H. Zhu and Z. Guo, *Chem. Sci.*, 2021, **12**, 9885–9894.
91 X. Kong, M. Li, B. Dong, Y. Yin, W. Song and W. Lin, *Anal. Chem.*, 2019, **91**, 15591–15598.
92 X. Li, Y. Pan, H. Chen, Y. Duan, S. Zhou, W. Wu, S. Wang and B. Liu, *Anal. Chem.*, 2020, **92**, 5772–5779.
93 L. Shi, C. Yan, Y. Ma, T. Wang, Z. Guo and W. H. Zhu, *Chem. Commun.*, 2019, **55**, 12308–12311.
94 R. Long, C. Tang, Z. Yang, Q. Fu, J. Xu, C. Tong, S. Shi, Y. Guo and D. Wang, *J. Mater. Chem. C*, 2020, **8**, 11860–11865.
95 D. Xiao, M. Jiang, X. Luo, S. Liu, J. Li, Z. Chen and S. Li, *ACS Sustainable Chem. Eng.*, 2021, **9**, 4139–4145.
96 X.-M. Cai, Y. Lin, Y. Li, X. Chen, Z. Wang, X. Zhao, S. Huang, Z. Zhao and B. Z. Tang, *Nat. Commun.*, 2021, **12**, 1773.
97 X. Zhang, C. Ren, F. Hu, Y. Gao, Z. Wang, H. Li, J. Liu, B. Liu and C. Yang, *Anal. Chem.*, 2020, **92**, 5185–5190.
98 S. M. Stanford and N. Bottini, *Nat. Rev. Drug Discovery*, 2023, **22**, 273–294.
99 X. Gao, G. Ma, C. Jiang, L. Zeng, S. Jiang, P. Huang and J. Lin, *Anal. Chem.*, 2019, **91**, 7112–7117.
100 L. Li, J. Ge, H. Wu, Q. H. Xu and S. Q. Yao, *J. Am. Chem. Soc.*, 2012, **134**, 12157–12167.